1-1-2011

Coordinated utilisation of wind farm reactive power capability for system loss optimisation

Lasantha Meegahapola
University of Wollongong, lasantha.meegahapola@rmit.edu.au

S Durairaj
Department of Electrical and Electronic Engineerin, rajsdr@rediffmail.com

D Flynn
University College Dublin, damian.flynn@ucd.ie

B Fox
The Queen's University of Belfast, b.fox@ee.qub.ac.uk

Coordinated utilisation of wind farm reactive power capability for system loss optimisation

Abstract

Most wind farms currently being installed are based upon doubly fed induction generator (DFIG) or direct-drive synchronous generator (DDSG) technology. Given that one of the impacts of introducing distributed generation is an alteration of steady-state power flows and voltages, both technologies are capable of providing local voltage support. Wind farms may, therefore, be included in optimal power flow (OPF) calculations to minimise fuel cost and/or network losses. The IEEE 30-bus system is considered as a case study, comparing fixed-speed induction generator (FSIG) requirements with DFIG capability. Results are presented for a range of DFIG capability modes, at varying system load and wind farm penetration levels. A significant reduction in losses can be achieved by suitable co-ordination of DFIG reactive power import/export, operating within typical grid code specifications. It is shown that the dynamic variability of reactive power requirements is readily accommodated by the power system. Finally, implementation options for the scheme and incentivising strategies are considered.

Keywords

utilisation, wind, farm, reactive, power, capability, system, loss, optimisation, coordinated

Disciplines

Physical Sciences and Mathematics

Publication Details

L. Meegahapola, S. Durairaj, D. Flynn & B. Fox, "Coordinated utilisation of wind farm reactive power capability for system loss optimisation," European Transactions on Electrical Power, vol. 21, (1) pp. 40-51, 2011.

Coordinated Utilisation of Wind Farm Reactive Power Capability for System Loss Optimisation

L. Meegahapola[1], S. Durairaj[2], D. Flynn[3] and B. Fox[1]

[1] The Queen's University of Belfast, School of Electronics, Electrical Engineering and Computer Science, Belfast BT9 5AH, N. Ireland, UK

[2] Kalasalingam University, Department of Electrical and Electronic Engineering, Tamil Nadu, India

[3]University College Dublin, Electricity Research Centre, School of Electrical, Electronic and Mechanical Engineering, Belfield, Dublin, Ireland

Abstract

Most wind farms currently being installed are based upon doubly-fed induction generator (DFIG) or direct-drive synchronous generator (DDSG) technology. Given that one of the impacts of introducing distributed generation is an alteration of steady-state power flows and voltages, both technologies are capable of providing local voltage support. Wind farms may, therefore, be included in optimal power flow calculations to minimise fuel cost and/or network losses. The IEEE 30-bus system is considered as a case study, comparing fixed-speed induction generator (FSIG) requirements with DFIG capability. Results are presented for a range of DFIG capability modes, at varying system load and wind farm penetration levels. A significant reduction in losses can be achieved by suitable co-ordination of DFIG reactive power import/export, operating within typical grid code specifications. It is shown that the dynamic variability of reactive power requirements is readily accommodated by the power system. Finally, implementation options for the scheme and incentivising strategies are considered.

Keywords:

Doubly-fed induction generator (DFIG), dynamic loss reduction, fixed-speed induction generator (FSIG), interior point algorithm, optimal power flow, reactive power dispatch

1. Introduction

Most wind farms now being installed are of the variable-speed type [1]. Whether they are based on doubly-fed induction generators (DFIGs) or on direct-drive synchronous generators (DDSGs), it is possible to vary reactive power import/export within the volt-ampere rating of the individual wind turbine generators (WTGs). The resulting wind farm is often connected at transmission or sub-transmission level. From an operational perspective, the wind farm is a small power station, with

active power determined by current wind conditions, and reactive power that may be controlled to achieve overall system objectives.

The determination of optimal power system steady-state operating conditions is the well-known optimal power flow (OPF) problem [2-3]. The OPF is a non-linear optimisation problem with constraints. Normally, the function to be minimised is the cost of operating the available generating plant or the summed network losses. The transmission system is modelled by the familiar Newton-Raphson power flow equations [4]. The solution of these non-linear equations enforces sufficient generation to supply the demand and losses. However, the OPF differs from a load flow calculation in that generator node quantities – active power, P, and voltage, V – are now independent variables with defined ranges. The OPF seeks to determine those values of P and V that minimise operating cost (or network losses). There may also be other variables which can be adjusted, in particular transformer tap ratios. An essential feature of OPF is that the dependent quantities, such as load voltages and line flows, must lie within defined ranges. The OPF solution must therefore conform to the Karush-Kuhn-Tucker (KKT) conditions of optimality [5].

While commercial OPF packages have been available for some years, the solution techniques continue to evolve. OPF is a mixed-integer, non-linear optimisation problem: integer variables appear in the mathematical formulation as discrete transformer tap positions, shunt capacitor bank switching, etc. Many analytical techniques have been proposed to solve the OPF problem including the gradient method [6], the Newton method [7], linear programming [8] and the interior point method [9-10]. More recent work has focussed on the use of artificial intelligence techniques such as fuzzy logic, genetic algorithms and evolutionary computing [11-13]. In the present work, the authors have used an iterative interior-point algorithm based on the Newton-Lagrange method [14].

The purpose of the work reported here is twofold. Firstly, to demonstrate the reactive power capabilities of various wind generation technologies, i.e. FSIG, DFIG, and DDSG, within the ambit of overall power system optimisation. Secondly, to show that such action is capable of delivering reduced system losses, and hence fuel savings, while maintaining a satisfactory network voltage profile under various system operating conditions. The paper will explain how a wind farm with reactive power control capability can be included within the OPF formulation. It will be shown how the WTG volt-ampere limits and grid code requirements can be incorporated. The paper will then go on to demonstrate the benefits of including wind generation within OPF for the standard IEEE 30-bus network, with four distributed wind farms each supplying up to 3.25% and 13% of the nominal demand.

2. Problem Formulation

2.1 Interior Point Algorithm

Interior point methods (IPM) are widely used in optimisation problems due to their fast convergence [14]. There are several variants of IPM, and this work incorporates the iterative infeasible primary-dual interior point algorithm based on the Newton-Lagrange method. Any optimisation problem can be represented as an objective function to be optimised subject to equality and inequality constraints as follows:

$$\begin{aligned} &\textit{Minimise} && f(\mathbf{x}) \\ &\textit{Subject to} && g(\mathbf{x}) = 0 \\ & && h(\mathbf{x}) \le 0 \end{aligned} \tag{1}$$

In an optimal power flow problem, the objective function $f(\mathbf{x})$ can be a function representing the transmission losses or generator fuel cost. The state vector $\mathbf{x}$ represents the system states such as voltage magnitudes, phase angles, active and reactive powers of generators, etc. The equality constraints generally are the load flow equations, while the inequality constraints correspond to system operating limits such as voltage limits, generator active power limits, etc.

As the first step, all the inequality constraints in (1) are transformed to equality constraints by the addition of slack variables, and the non-negative constraints are then replaced by the logarithmic barrier function. This implicitly imposes positive conditions for the slack variables ($\mathbf{s}$) which then can be represented in the following way while incorporating the objective function.

$$\begin{aligned} &\textit{Minimise} && f(\mathbf{x},\mathbf{s},\mu) = f(\mathbf{x}) - \mu\sum_{j=1}^{n}\ln(s_j) \\ &\textit{Subject to} && g(\mathbf{x}) = 0 \\ & && h(\mathbf{x}) + \mathbf{s} = 0 \end{aligned} \tag{2}$$

The penalty weighting factor μ is decreased iteratively from a defined maximum to a minimum (zero is the theoretical minimum) during the iterative optimisation process. The Lagrangian function can then be derived from equation (2) and represented as follows:

$$\textit{Minimise} \quad L(\mathbf{x},\mathbf{s},\mu) = f(\mathbf{x}) - \mu\sum_{j=1}^{n}\ln(s_j) - \boldsymbol{\lambda}^T \bullet g(\mathbf{x}) + \boldsymbol{\pi}^T \bullet (h(\mathbf{x}) + \mathbf{s}) \tag{3}$$

The stationary point of the Lagrangian function represents the optimal solution of the sub-problem, which should fulfil the required first-order KKT conditions [15].

$$
\begin{aligned}
\nabla_x L(\mathbf{x},\mathbf{s},\mu) &= \nabla f(\mathbf{x}) - \nabla g(\mathbf{x})^T \boldsymbol{.}\boldsymbol{\lambda} + \nabla h(\mathbf{x})^T \boldsymbol{.}\boldsymbol{\pi} &= 0 \quad \text{(a)} \\
\nabla_\lambda L(\mathbf{x},\mathbf{s},\mu) &= -g(\mathbf{x}) &= 0 \quad \text{(b)} \\
\nabla_\pi L(\mathbf{x},\mathbf{s},\mu) &= h(\mathbf{x}) + \mathbf{s} &= 0 \quad \text{(c)} \\
\nabla_s L(\mathbf{x},\mathbf{s},\mu) &= -\boldsymbol{\mu}\boldsymbol{.}\mathbf{S}^{-1}\boldsymbol{.}\mathbf{e} + \boldsymbol{\pi} &= 0 \quad \text{(d)}
\end{aligned}
\tag{4}
$$

S is a diagonal matrix consisting of components of **s**, **e** is a matrix of ones with appropriate dimensions (**e** = $[1,\ldots,1]^T$), and **μ** is a matrix consisting of components of μ. Equation (4-d) can be transformed and represented as a complementary slackness condition as follows:

$$
\mathbf{S}\boldsymbol{.}\boldsymbol{\Pi}\boldsymbol{.}\mathbf{e} = \boldsymbol{\mu}\boldsymbol{.}\mathbf{e} \tag{5}
$$

Π is a diagonal matrix consisting of components of π. Newton's method is then applied by taking the first derivatives of equations (4-a)-(4-c) and (5), and the following symmetrical system can be obtained.

$$
\begin{bmatrix} -\mathbf{H} & \nabla g(\mathbf{x})^T & -\nabla h(\mathbf{x})^T & 0 \\ \nabla g(\mathbf{x}) & 0 & 0 & 0 \\ -\nabla h(\mathbf{x}) & 0 & 0 & -\mathbf{I} \\ 0 & 0 & \mathbf{I} & \mathbf{S}^{-1}\boldsymbol{.}\boldsymbol{\Pi} \end{bmatrix} \boldsymbol{.} \begin{bmatrix} \Delta\mathbf{x} \\ \Delta\boldsymbol{\lambda} \\ \Delta\boldsymbol{\pi} \\ \Delta\mathbf{s} \end{bmatrix} = - \begin{bmatrix} \nabla_x L \\ \nabla_\lambda L \\ \nabla_\pi L \\ \nabla_s L \end{bmatrix} \tag{6}
$$

The Hessian matrix (**H**) consists of second-order partial derivatives of the objective function. The gradient of the penalty weighting factor (μ) tends to zero, since the KKT system was solved for a fixed penalty factor. The derived equation (6) identifies the direction of the new optimal point in the solution space, while the following equations are used to update the variables before the next iteration.

$$
\begin{aligned}
\mathbf{x}^{k+1} &= \mathbf{x}^k + \alpha_0 \boldsymbol{.} \alpha_P \boldsymbol{.} \Delta\mathbf{x} \\
\mathbf{s}^{k+1} &= \mathbf{s}^k + \alpha_0 \boldsymbol{.} \alpha_P \boldsymbol{.} \Delta\mathbf{s} \\
\boldsymbol{\lambda}^{k+1} &= \boldsymbol{\lambda}^k + \alpha_0 \boldsymbol{.} \alpha_D \boldsymbol{.} \Delta\boldsymbol{\lambda} \\
\boldsymbol{\pi}^{k+1} &= \boldsymbol{\pi}^k + \alpha_0 \boldsymbol{.} \alpha_D \boldsymbol{.} \Delta\boldsymbol{\pi}
\end{aligned}
\tag{7}
$$

In order to update the variables it is essential to determine the size of the primary and dual steps, which can be accomplished using the following equations:

$$
\begin{aligned}
\alpha_P &= \min\left[\min_{\Delta s_j < 0} \frac{s_j}{|\Delta s_j|}, 1 \right] \\
\alpha_D &= \min\left[\min_{\Delta \pi_j < 0} \frac{\pi_j}{|\Delta \pi_j|}, 1 \right]
\end{aligned}
\tag{8}
$$

Using the updated variables and penalty weighting factor, the optimisation problem will revert to equation (3), which will solve the Newton equations until the predefined error factor is met. The optimisation problem will successfully converge if either of the following conditions is satisfied.

I. All load flow constraint equations ($g(\mathbf{x}) = 0$ and $h(\mathbf{x}) < 0$) are fulfilled to a predefined degree of exactness (i.e. within an allowable tolerance).
II. The Lagrangian function $L(\mathbf{x}, \mathbf{s}, \mu)$ converges. This can be achieved if either the objective function itself converges to a stationary point, or the gradient of the objective function converges to zero.

The optimisation process starts by initialising the starting configuration of the system, determined here through a load flow solution. It has been found that the optimum solution can be obtained within 6 or 7 iterations.

2.2 Operating Characteristics of Wind Farms

Wind farms employ mainly fixed-speed induction generators (FSIG) or doubly-fed induction generators (DFIG). A FSIG wind farm consists of multiple FSIG wind turbines, each with its own reactive power requirements, dependent on wind speed (active power) and local voltage. A capacitor bank is placed at each FSIG busbar node providing fixed no-load reactive power compensation (Q_{cap}) to ensure compliance with grid code standards. Figure 1 illustrates how the reactive power requirement of a FSIG depends on active power generation.

In the case of a DFIG wind farm it is assumed that active power depends on wind speed, while reactive power is a controlled variable [16]. Reactive power is controlled using the DFIG's rotor-side voltage source converter, rated typically at 25% of the generator rating. The reactive power capability of DFIGs is not well defined, and varies between different manufacturers, but grid codes generally require that a wind farm is capable of operating from 0.95 lagging to 0.95 leading power factor at full active power output [17]. The potential therefore exists for continuous voltage regulation in response to variations in load behaviour, external faults, etc. [18]. Furthermore, since a DFIG is considered as a controllable PQ source, the presented results are equally applicable to full-converter (synchronous machine) wind turbines. Various operating charts have been derived in the literature for DFIGs based on technical constraints [19], i.e. stator and rotor current limits. Here it is assumed conservatively that the DFIG complies with the typical grid code requirement illustrated in Figure 2.

The reactive power limits considered in turn at the wind farm nodes are one of the following: ±0.329 pu (equivalent to a power factor of 0.95 at rated active power export); ±0.203 pu (equivalent to a power factor of 0.98 at rated active power export); and unlimited reactive power. Reactive power imports are represented as negative (leading) quantities, while reactive power exports are expressed as positive (lagging) quantities.

2.3 Loss Minimisation with Wind Generation

The objective here is to minimise the active power loss in the network. The following equation is defined as the objective function for loss minimisation.

$$F = \sum_{\substack{k \in N_b \\ k=(i,j)}} g_k (U_i^2 + U_j^2 - 2U_i U_j \cos \theta_{ij}) \tag{9}$$

Regardless of the objective function, however, an OPF must ensure that the entire set of voltage and power constraints are satisfied. Various categories of constraints exist, and these distinct categories are described below.

2.3.1 Equality constraints

The transmission network is modelled by a power balance equation at each node. The algebraic sum of the active and reactive powers injected into each node *i* must equal zero:

$$\begin{aligned} P_i - U_i \sum_{j=1}^{N_B} U_j \left(G_{ij} \cos\theta_{ij} + B_{ij} \sin\theta_{ij} \right) = 0 \\ Q_i - U_i \sum_{j=1}^{N_B} U_j \left(G_{ij} \cos\theta_{ij} - B_{ij} \sin\theta_{ij} \right) = 0, \quad i \in N_B \end{aligned} \tag{10}$$

In addition, the following equality constraint was formulated to ensure that all the available wind generation (P_{wind}) at a particular instant is generated by the wind farms installed in the network during the optimisation.

$$\sum_{i=1}^{N_W} P_{WG_i} = P_{wind} \ , \ i \in N_W \tag{11}$$

2.3.2 Inequality constraints

The active power of the wind generating units are set according to equation (11). However, as explained earlier, FSIG reactive power output depends on the active power generation, and is therefore beyond the scope of the OPF optimisation problem. By contrast, DFIG reactive power output (Q_{DFIG}) can be controlled, and the following inequality constraint can be included within the OPF framework, based on the grid code requirement for a power factor range of 0.95 leading to 0.95 lagging.

$$-0.329 \text{ pu} \le Q_{DFIG} \le 0.329 \text{ pu} \tag{12}$$

The conventional generating units have maximum and minimum generating limits, both in active and reactive power, beyond which it is not feasible to generate for technical or economic reasons.

$$P_{g_i}^{\min} \le P_{g_i} \le P_{g_i}^{\max}$$
$$Q_{g_i}^{\min} \le Q_{g_i} \le Q_{g_i}^{\max} \quad i \in N_G \tag{13}$$

Voltage limits constrain bus voltages (V_i) to remain within an allowable range. Our assumption here is that node voltages are maintained between 0.95 pu and 1.05 pu.

$$0.95\,\text{pu} \le U_i \le 1.05\,\text{pu}, \; i \in N_B \tag{14}$$

2.4 Test System Formulation

The above problem formulation was applied to the standard IEEE 30-bus system, which operates at fixed tap positions and with relaxed branch flow limits – see Figure 3. The formulated OPF problem was then solved using the steps shown in equations (2) to (8) until the defined criterion was met.

The simulation study was carried out using the DIgSILENT Power Factory software [20] to perform the optimal power flow. The nominal system load is 283.4 MW, supplied by 6 generators located at nodes 1, 2, 5, 8, 11 and 13. The existing system was modified by introducing 4 wind farms. Bearing in mind that wind farms are usually located in remote areas of a network, LV nodes 10, 14, 18 and 30 have been selected for this study. It was noted that bus 30 is the weakest bus of this system [21]. Each FSIG has a capacity of 2.3 MW, with induction machine parameters based on commercial implementations [22]. For convenience within DIgSILENT, each DFIG wind farm was represented as a single synchronous machine, controlled within a PQ operating chart, as indicated in Figure 2. Such a representation is appropriate, since the internal electrical quantities of the DFIG do not influence the optimisation process. For clarity, each wind farm is assumed to provide a fixed proportion of the total wind generation. It was noted that the network voltage limits are not violated even when the system load is doubled. Consequently, the fixed capacitors at buses 10 and 24 were removed. Hence, the algorithm, as implemented, contains no integer variables. When more wind generation is added to the network, the conventional generation capacity is reduced, starting from the most heavily loaded unit since it contributes most to the losses, and subsequently other generator units also reduce their output until the lower limit is reached. The upper and lower limits of generator active and reactive power are taken from [6] and are given in Table 1.

Both cost and loss minimisation were applied to the IEEE 30-bus system. It was found that the losses were slightly greater when the cost was minimised, as would be expected. However, the trends presented later were similar, regardless of whether cost or loss minimisation was used. It was decided to apply loss minimisation, as defined by equation (9), to focus attention on DFIG reactive power adjustment as a means of minimising active losses subject to voltage constraints.

3. Loss Minimisation with Variable Wind Conditions

3.1 Smaller (4 × 9.2 MW) Wind Farm Installed Capacity

Initially, 9.2 MW (2.3 MW × 4 turbines) FSIG/DFIG wind farms were sited at the 4 locations on the test system. The system load was varied from the nominal demand (283.4 MW) by ±10%, and optimal power flows were performed to minimise network losses for a range of wind farm outputs from 0 - 9.2 MW. DFIG reactive power was limited to 0.329 pu import/export, as outlined in Figure 2. For the zero wind condition it was assumed that DFIGs can operate as STATCOMs, providing voltage support, as necessary, while any FSIGs are disconnected from the network. For convenience, it was assumed that wind speed is uniform within a particular wind farm and across sites, so that the active power output of each wind farm was identical for a particular loading condition. Similarly, any variation in the aerodynamic efficiency of variable-speed DFIGs in comparison with FSIGs was ignored. Figure 4 illustrates the variation in network losses for both FSIG/DFIG wind farms for a range of wind farm outputs and system loading.

The system losses were determined as the transmission losses (including transformer losses) of the system, excluding internal generator losses. It can be clearly seen that as wind farm output is increased, network losses are reduced. So, for example, at 100% system loading with DFIG wind farms, the losses decrease from 4.83 MW at zero wind farm output to 3.12 MW with the 4 wind farms at full output, a 35% reduction. As wind farm output increases, more of the load is being supplied by local wind farms, thus reducing power flow and associated losses in the HV network. Similarly, as the system load is raised to 110% of nominal (311.7 MW), the network losses naturally increase, but the distributed wind farms provide a more significant reduction in losses, 6.90 MW to 4.16 MW, for the same reason as before.

It can also be seen that the network loss for DFIG-based wind farms is slightly lower than that for FSIG-based wind farms. Figure 5 depicts the loss reduction for DFIG installations as a fraction of the FSIG losses for each system condition, and is defined as follows:

$$\%\ \ Loss\ \ reduction = \frac{L_{FSIG} - L_{DFIG}}{L_{FSIG}} \times 100 \tag{15}$$

As wind farm output increases, the benefit of DFIGs with control of reactive power export becomes more evident. So, at 110% system loading, the loss reduction increases from 1.9% to 5.0% between minimum and maximum wind farm output. The absolute loss reduction, however, remains almost constant, irrespective of system load and wind farm output.

For the 100% load condition, Figure 6 illustrates the reactive power output variations for both FSIG and DFIG wind farms at the 4 wind farm locations. For the FSIG wind farms, reactive power import

(negative quantity) increases with active power export, as would normally be expected. The power factor correction (PFC) capacitance placed at each wind farm is sized for no-load compensation at 1 pu voltage, so that the *net* reactive power import at each location will depend on local voltage. For the DFIG wind farms, the reactive power control actions of each wind farm proposed by the OPF are slightly different. The DFIG located at bus 18 is restricted by its reactive power export (positive) limit of 3.03 MVAr (0.329 pu). For the remaining DFIGs, the reactive power export actually decreases between no wind and maximum active power, especially for buses 14 and 30. This is not surprising, given that the voltage at a generation node will tend to rise with active power export, particularly in network areas where the transmission line X/R ratio is low [23]. Reducing the reactive power export with increasing wind farm generation ensures that network voltages remain within limits – for the candidate nodes, a maximum voltage of 1.04 pu occurs at bus 14 at a wind farm output of 9.2 MW (not shown).

3.2 Larger (4 × 36.8 MW) Wind Farm Installed Capacity

If the wind farm capacity at each node is now increased to 36.8 MW (2.3 MW × 16 turbines), the optimal power flows can be repeated. Figure 7 illustrates the variation in network losses for both FSIG and DFIG wind farms as the system load is varied by ±10% and the active power at each wind farm varies between minimum and maximum output.

At low wind farm outputs, the system losses gradually decrease as before, as the system load is increasingly supplied by local (wind) generation. However, losses are minimised at a certain common wind farm output, and beyond this threshold network losses increase fairly rapidly, as the wind farms now *export* active power to the rest of the system. The exact threshold will depend on system demand, increasing from approximately 10, 15 and 20 MW at each wind farm as the system load is set at 90%, 100% and 110% of nominal load.

Figure 8 illustrates the reactive power output for the FSIG and DFIG wind farms. The FSIG reactive power profile is similar to Figure 6-a, with the wind farm at bus 14 requiring most reactive power import. The voltage at bus 14 is noticeably higher than at the other buses (not shown), and at higher wind farm output is limited to the upper voltage threshold (1.05 pu). For the DFIG scenario, reactive power export at bus 10 (rather than bus 18) is now the limiting factor, with the wind farm at this location operating at its maximum capability of 12.11 MVAr (0.329 pu). For the remaining wind farms, reactive power export tends to decrease with increased active power output, limiting any voltage rise. Indeed, at bus 14 the DFIG exports reactive power at low wind farm output, before importing reactive power at higher wind farm outputs, in order to maintain the voltage at bus 14 below the limit: see Figure 9.

3.3 DFIG Reactive Power Capability

So far it has been assumed that the rotor-side converter of each DFIG can support reactive import/export equivalent to ±0.95 power factor at full active power generation. Two additional scenarios are of interest: a DFIG with limited reactive power capability (±0.98 pf), and a DFIG with unlimited reactive power capability. The latter case is impracticable, but provides an indication of whether additional reactive power capability is of value.

Figure 10 illustrates the impact on losses of the four 36.8 MW wind farms, comparing DFIGs with unlimited reactive power capability to converters limited to ±0.95 pf rating. For the unrestricted case, at maximum wind farm output, the active power loss is slightly reduced (from 5.46 MW to 5.41 MW at 100% loading), but the overall benefit is clearly minimal.

Similar results are obtained if the converter rating is restricted to ±0.98 pf at full active power export (5.71 MVAr at 100% loading). The network voltages tend to be slightly higher as the reactive power limits are relaxed, with buses 14 and 30 close to the upper voltage limit for high wind conditions. The only major difference is that the reactive power export at bus 10 ranges from 7.5, to 12.1 and to 29.7 MVAr, corresponding to ±0.98 pf, ±0.95 pf and unlimited converter rating.

If Figures 7 and 10, showing the system losses for FSIG, ±0.95 pf DFIG and unconstrained DFIG (uDFIG) are combined, the loss reduction for the three cases can be compared. Adopting the same form as equation (15), the loss reduction can be calculated as follows:

$$\%\ Loss\ \ reduction\,(DFIG\ v\ FSIG) = \frac{L_{FSIG} - L_{DFIG}}{L_{DFIG}} \times 100$$

$$\%\ Loss\ \ reduction\,(uDFIG\ v\ DFIG) = \frac{L_{DFIG} - L_{uDFIG}}{L_{DFIG}} \times 100 \qquad (16)$$

Figure 11 compares the loss reduction for (4 × 36.8) MW of 0.95 pf DFIG wind farm capacity relative to FSIG and uDFIG technology. In comparing FSIG and DFIG implementations, the loss reduction is slightly skewed by the parabola-shaped system loss characteristics of Figure 7 and 10. Consequently, DFIGs tend to offer maximum benefit when wind farm active power output is such that network losses are minimised, depending on system loading. An average reduction in losses of 8-10% can be seen across the system loading and wind farm operating ranges. However, when DFIGs are replaced by unconstrained DFIGs, the benefits are less clear, with approximately 1% reduction in losses for all load conditions and wind farm outputs. These results suggest that loss reduction does not justify extending DFIG reactive power capability.

4. Dynamic Network Loss Minimisation

The analysis presented so far has considered *static* network loss minimisation for a particular power system incorporating different wind farm technologies. It is clear that DFIGs provide the capability to control local voltage and reduce network losses. However, it is also important to understand the *dynamic* variation of network voltages and reactive power import/export which may be required in practice to achieve the desired optimisation objective. System demand and wind generation output data for a 24-hour period, at 1-hour intervals, have been selected for a particular winter day on the Ireland power system [24], Figure 12. The nominal (100%) system load is taken as the average demand for the selected day, while 100% wind generation is based upon the maximum recorded wind generation for the Ireland system. For convenience of OPF analysis, the demand profile has been quantised in 5% load increments.

Adopting the above demand and wind profiles, optimal power flow is performed for 4 × 9.2/36.8 MW, FSIG/DFIG technology at the existing wind farm locations on the IEEE 30 bus system. The DFIG wind farms operate with a ±0.95 pf converter rating. The variation in system losses for FSIG and DFIG wind farms is shown in Figure 13.

Considering first the 4 × 9.2 MW FSIG/DFIG wind farms: during periods of low demand, for example 2-7 am, system losses are reduced, as *high* wind farm output is sufficient to meet local load requirements. Later in the day, for example 5-9 pm, when the system demand is at its peak, wind farm output is comparatively low, so that most of the load must be supplied by conventional generation on the distant HV network. Hence, network losses are high.

Considering now the 36.8 MW installations, a different pattern is obtained. In the early morning, network losses are at their peak, as now the high wind farm output exceeds the local load requirement and active power is exported to other parts of the network. Later in the day, even though wind farm output is less, much of the local demand can be supported and network losses are reduced. Overall, the variation in losses across the day is less significant for the 36.8 MW wind farms than for the 9.2 MW installations, and DFIG wind farms consistently offer reduced system losses compared with their FSIG equivalents.

The corresponding variations in voltage and reactive power at bus 14 for the various scenarios are shown in Figure 14. For the 9.2 MW wind farms, the FSIG and DFIG voltage profiles are similar, offset from each other by approximately 0.004 pu at all times. If desired, therefore, the FSIG voltage profile could be optimised by increasing the PFC capacitance at node 14. Despite the variations in system load and wind generation the voltage variation is small, ranging from 1.030 – 1.038 pu for the FSIG wind farm, for example. The corresponding variation in reactive power

import/export for both FSIG and DFIG wind farms is minimal, varying slightly in sympathy with the system demand. For the 36.8 MW wind farms, the voltage remains close to the voltage limit of 1.05 pu. It is only when the wind farm contribution to total generation decreases, 0-3 am and 7-9 pm, that the voltage begins to fall. However, in order for the DFIG at bus 14 to maintain the voltage within limits, the reactive power export/import varies noticeably throughout the day, although well within the permitted limits of ±12.11 MVAr (0.329 pu). When wind generation is at its minimum, 0-2 am, the DFIG exports reactive power, boosting the local voltage. But for the remainder of the day the DFIG imports reactive power, as a mirror image of the wind profile, in order that the voltage limit is not exceeded. This is particularly necessary at around 6 am when system demand is at its lowest and wind generation, coincidentally, is at its peak.

The voltage and reactive power variations at buses 10, 14, 18 and 30 are summarised in Tables 2 and 3, corresponding to the 4 × 9.2 MW and 4 × 36.8 MW installations. Similar to bus 14, it can be seen that the voltage variations at buses 10 and 18 for FSIG and DFIG modes are relatively small, approximately 0.01 pu. The voltage variation at bus 30, the weakest bus, is significantly more than at the other locations.

5. Discussion

The results assume that fixed-speed induction generators have fixed shunt capacitive compensation, set to reduce no-load reactive power consumption to zero. In fact, some manufacturers provide several steps of capacitive compensation as active power, and hence the induction generator reactive power requirement, increases [23], the aim being to approach unity power factor at all loads. Thus the loss reduction achieved by DFIG technology may be less significant in practice than the above results suggest. However, the results for DFIG based wind farms indicate that optimum wind farm reactive power generation varies with location and system loading. For example, the four wind farm reactive power generations depicted in Figure 8-b range from a fixed export over the load range (bus 10) to increasing import (bus 14). The results as a whole show that the OPF approach utilises DFIG reactive power capability in a way that is sympathetic to the changing network requirements. It should be noted that this flexibility may sacrifice loss reduction in favour of satisfying voltage limits – as was the case for bus 14 (Figures 8-b and 9).

The proposed approach requires regular OPF calculations, and communications to reset the wind farm reactive power generations, probably for each trading period. Alternatively, OPFs could be computed off-line for a range of system demands and wind power generations, with the real-time values obtained by interpolation. In either case, the reactive power adjustment can be based on recent wind farm generation data, obviating the need for long-term wind power forecasting. Transmission system operators can already curtail the active power of newer wind farms [25].

Hence the procedure and infrastructure to support centralised reactive power control for wind farms is likely to become more common [26].

The results show that there is an economic benefit in controlling wind farm reactive power. The benefit is acknowledged in Spain, for example, where wind farms qualify for a bonus of up to 8% for operating at a desirable power factor from 0.95 leading to 0.95 lagging at peak, normal and valley periods [27-29]. True allocation of the costs and benefits of transmission losses to generators is a challenging market issue beyond the scope of this paper [28]. However, while research on the issue continues, market operators can adopt an approximate, pragmatic approach. For example, wind farms could receive a reward/penalty based on the market value of the sector's impact on transmission losses, shared on the basis of reactive power capability.

6. Conclusions

It has been shown that DFIG based wind farms may be included in optimal power flow calculations. The objective, with or without wind farms, is to minimise losses while retaining node voltages and line currents within limits. In the case of DFIG based wind farms, only reactive power generations are available as control variables within the OPF.

The loss reduction available through adjustment of wind farm reactive power generation was assessed for the IEEE 30-bus network. The wind generation, in the form of wind farms at four nodes, corresponded to 13% and 53% of total conventional generating capacity. Relative to wind farms based on fixed-speed induction generators with fixed no-load capacitive compensation, DFIG based wind farms with OPF-derived reactive power generations resulted in loss reductions of 6% (4 × 9.2 MW) and 11% (4 × 36.8 MW) at full wind farm output. The reductions would probably be somewhat less if the comparison were with fixed-speed technology incorporating switched capacitive compensation.

The required range of DFIG reactive power capability to achieve the loss reductions was examined. It was found that the standard DC-link rating of 25% of the generating unit capacity provided ample scope for loss reduction. Hence there is little justification for increasing the DC-link rating for reasons of loss minimisation.

The behaviour of the DFIG capacity under OPF control was examined over a typical 24 hour period. It was found that the wind generation energy, corresponding to 10.1% of the demand (4 × 9.2 MW), delivered an additional 2.2% of loss reduction with OPF-controlled DFIG capacity relative to fixed-speed technology. The corresponding figure for the higher level of wind generation (4 × 36.8 MW) was 4.7%.

Acknowledgements

The authors wish to acknowledge the financial support provided by the Department of Science and Technology, India and the Department of Communications, Energy and Natural Resources, Ireland under the Strategy for Science, Technology and Innovation (2006-2013). The views expressed in this study are the authors' own and do not necessarily reflect the views and opinions of the Minister for Communications, Energy and Natural Resources.

List of Symbols

$f(\mathbf{x})$, F	objective function
$g(\mathbf{x})$	equality constraints
$h(\mathbf{x})$	inequality constraints
$\mathbf{x}$	state vector
$\mathbf{s}$	slack variable vector
n	number of inequality constraints
μ	penalty weighting factor
$\boldsymbol{\lambda}$, $\boldsymbol{\pi}$	Lagrangian multipliers
$\nabla g(\mathbf{x})$	matrix of the gradient vectors of the equality constraints
$\nabla h(\mathbf{x})$	matrix of the gradient vectors of the inequality constraints
$\mathbf{e}$	matrix of appropriate dimension with ones
$\mathbf{H}$	Hessian matrix
$\mathbf{S}$	diagonal matrix defined by the components of $\mathbf{s}$
$\mathbf{\Pi}$	diagonal matrix defined by the components of π
$\mathbf{I}$	identity matrix
α_P, α_D	primary and dual step size
α_0	safety factor
Q_{cap}	no-load capacitive reactive power compensation
P_i, Q_i	active and reactive powers injected into network at bus i
U_i, U_j	bus voltages at i and j
G_{ij}, B_{ij}	mutual conductance and susceptance between bus i and bus j
Pg_i, Qg_i,	active and reactive power of generator at bus i
θ_{ij}	voltage angle difference between bus i and bus j
g_k	conductance of branch k
N_B, N_b	number of buses and branches in the system
P_{WGi}	wind farm i power output
P_{wind}	total wind power
N_W, N_G	number of wind generators and conventional generators in the system
L_{FSIG}	system losses with FSIG
L_{DFIG}	system losses with DFIG
L_{uDFIG}	system losses with unconstrained DFIG
P_{gi}^{min}, P_{gi}^{max}	minimum and maximum active power limits of generator at bus i
Q_{gi}^{min}, Q_{gi}^{max}	minimum and maximum reactive power limits of generator at bus i

References

1. Hansen AD, Hansen LH. Wind turbine concept market penetration over 10 years (1995-2004). *Wind Energy* 2007; **10**(1):81-97.
2. Dommel HW, Tinney WF. Optimal power flow solutions. *IEEE Transactions on Power Apparatus and Systems* 1968; **87**(10):1866–1876.
3. Shen CM, Laughton MA. Determination of optimum power-system operating conditions under constraints. *Proceedings of the IEE* 1969; **116**(2):225–239.
4. Tinney WF, Hart CE. Power flow solution by Newton's method. *IEEE Transactions on Power Apparatus and Systems* 1967; **86**(11):1449–1460.
5. Wood AJ, Wollenberg BF. *Power generation, operation and control*. Wiley, 1996.
6. Alsac O, Stott B. Optimal load flow with steady state security. *IEEE Transactions on Power Apparatus and Systems* 1974; **93**(3):745-751.
7. Sun DI, Ashley B, Brewer B, Hughes A, Tinney WF. Optimal power flow by Newton approach. *IEEE Transactions on Power Apparatus and Systems* 1984; **103**(10):2864–2880.
8. Mangoli MK, Lee KY. Optimal real and reactive power control using linear programming. *Electric Power Systems Research* 1993; **26**(11):1–10.
9. Momah JA, Zhu JZ. Improved interior point method for OPF problems. *IEEE Transactions on Power Systems* 1999; **14**(3):1114–1120.
10. Wu YC, Debs AS, Marsten RE. A direct nonlinear predictor-corrector primal-dual interior point algorithm for optimal power flows. *IEEE Transactions on Power Systems* 1994; **9**(2):876-883.
11. Venkatesh B, Arunagiri A, Gooi HB. Unified OPF method for maximizing voltage stability margin using successive fuzzy LP. *Electric Power Systems Research* 2003; **64**(2):119-128.
12. Todorovski M, Rajicic D. An initialization procedure in solving optimal power flow by genetic algorithm. *IEEE Transactions on Power Systems* 2006; **21**(2):480-487.
13. Ongsakul W, Tantimaporn T. Optimal power flow by improved evolutionary programming. *Electric Power Components and Systems* 2006; **34**(1):79-95.
14. Andersen ED, Gondzio J, Meszaros C, Xu X. Implementation of interior-point methods for large-scale linear programming. *Technical Report* 1996.3, Logilab, University of Geneva, 1996.
15. Kuhn M. The Karush-Kuhn-Tucker Theorem. CDSEM, University of Mannheim, 2006.
16. Kayikci M, Milanovic JV. Reactive power control strategies for DFIG-based plants. *IEEE Transactions on Energy Conversion* 2007; **22**(2): 389-396.

17. Fox B, Flynn D, Bryans L, Jenkins N, Milborrow D, O'Malley M, Watson R, Anaya-Lara O. *Wind power integration: connection and system operational aspects*. IET Power and Energy Series 50, 2007.

18. Slootweg JG, de Haan SWH, Polinder H, Kling WL. Voltage control methods with grid connected wind turbines. *Wind Engineering* 2001; **25**(6):353-365.

19. Lund T, Sorensen P, Eek J. Reactive power capability of a wind turbine with doubly fed induction generator. *Wind Energy* 2007; **10**(4):379-394.

20. Power Factory manual, DIgSILENT Power Factory Version 13.2, GmbH, Germany, 2007.

21. El-Kateb MM, Abdelkader S, Kandil MS. Linear indicator for voltage collapse in power systems. *IEE Proceedings Part C* 1997; **144**(2):139-146.

22. El-Helow HM, Tennakon SB. Evaluation of fixed-speed wind turbine for large scale wind farms considering new UK grid code. *Renewable Energy* 2008; **33**(1):1-12.

23. Dinic N, Fox B, Flynn D, Xu L, Kennedy A. Increasing wind farm capacity. *IEE Proceedings Part C* 2006; **153**(4):493-498.

24. Eirgrid plc. Ireland transmission system operator, http://www.eirgrid.com [accessed June 2008].

25. Barry D, Smith P. Analysis of the integration of wind generation into the Irish system. *IEEE PowerTech*, St Petersburg, 2005.

26. Ackermann T. (Ed.). *Wind power in power systems*. Wiley, 2005.

27. Martinez E, Sanz F, Blanco J, Daroca F, Jimenez E. Economic analysis of reactive power compensation in a wind farm: influence of Spanish energy policy. *Renewable Energy* 2008; **33**(8):1880-1891.

28. Kirschen D, Strbac G. *Fundamentals of power system economics*. Wiley, 2004.

29. De Oliveira-De Jesus PM, Castronuovo ED, Ponce de Leao MT. Reactive power response of wind generators under an incremental network-loss allocation approach. *IEEE Transaction on Energy Conversion* 2008; **23**(2):612-621.

30. Durairaj S, Fox B. Optimal power flow under variable wind generation. *International Journal of Energy Technology and Policy* 2008; **6**(5):608-620.

Tables

Table 1: Generator Data

	Active Power (MW)		**Reactive Power (MVAr)**	
Bus no.	Lower limit	Upper Limit	Lower limit	Upper Limit
1	50	200	-20	250
2	20	80	-20	100
5	15	50	-15	80
8	10	35	-15	60
11	10	30	-10	50
13	12	40	-15	60

Table 2: Voltage and reactive power variations for 4 × 9.2 MW wind farms

Wind Farm	**Bus Voltage (pu)**		**Reactive Power (MVAr)**	
	FSIG	DFIG	FSIG	DFIG
10	1.002 – 1.010	1.003 – 1.012	-1.75 to -0.53	2.44 to 2.62
14	1.030 – 1.038	1.034 – 1.042	-1.8 to -0.65	1.6 to 1.87
18	1.002 – 1.028	1.009 – 1.020	-1.74 to -0.52	3.02
30	0.954 – 1.011	0.974 – 1.030	-0.4 to -1.75	2.1 to 3.0

Table 3: Voltage and reactive power variations for 4 × 36.8 MW wind farms

Wind Farm	**Bus Voltage (pu)**		**Reactive Power (MVAr)**	
	FSIG	DFIG	FSIG	DFIG
10	1.004 – 1.008	1.008 – 1.013	-6.7 to -2.1	12.11
14	1.040 – 1.049	1.044 – 1.049	-7.4 to -2.8	-4.4 to 1.4
18	1.018 – 1.025	1.032 – 1.042	-7.0 to -2.1	5.9 to 6.1
30	0.996 – 1.034	1.020 – 1.049	-1.45 to -3.65	1.1 to 2.7

Figure Titles

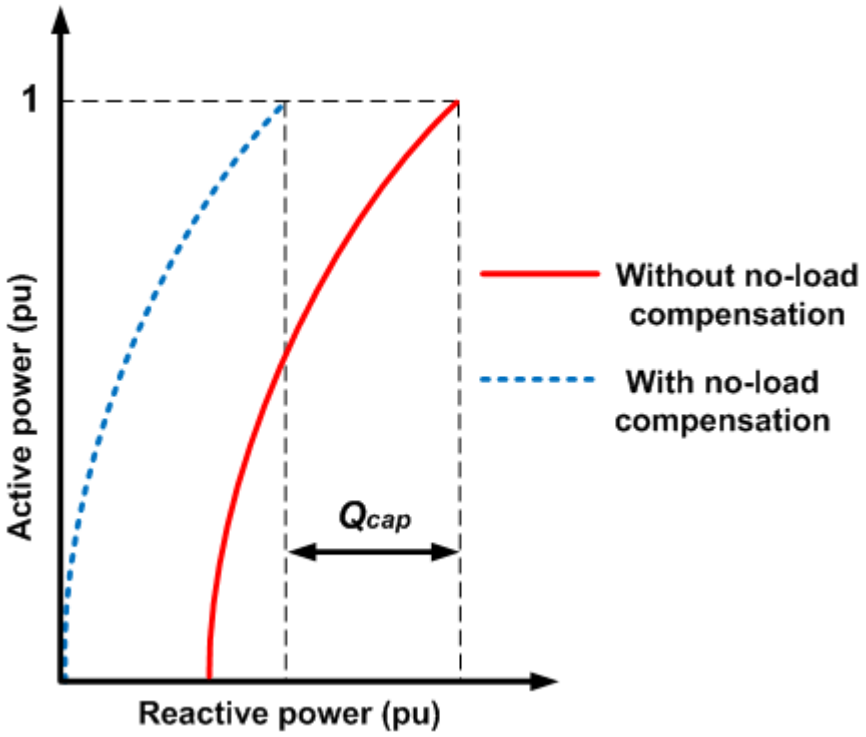

Figure 1: FSIG power characteristics

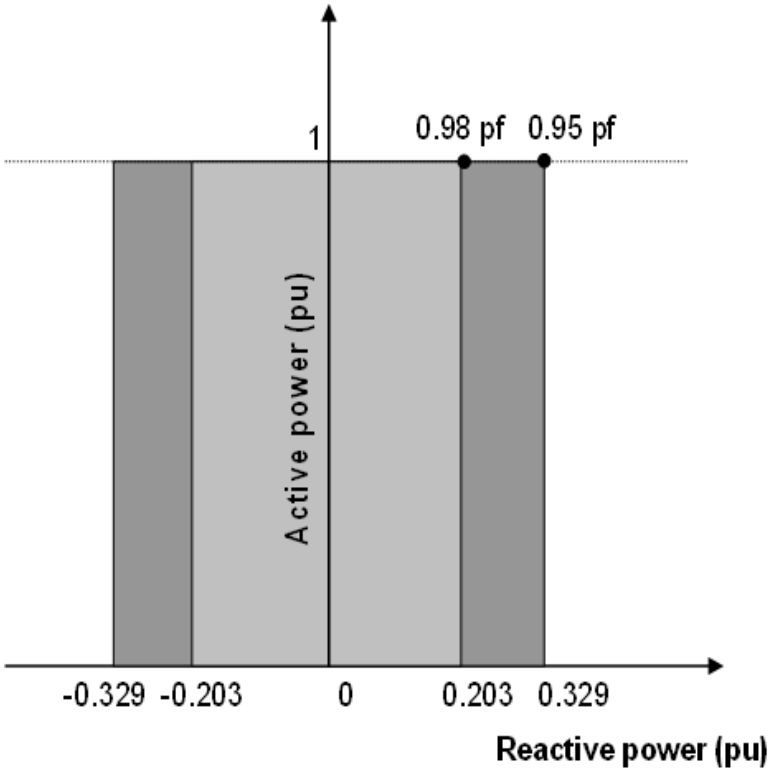

Figure 2: DFIG capability chart

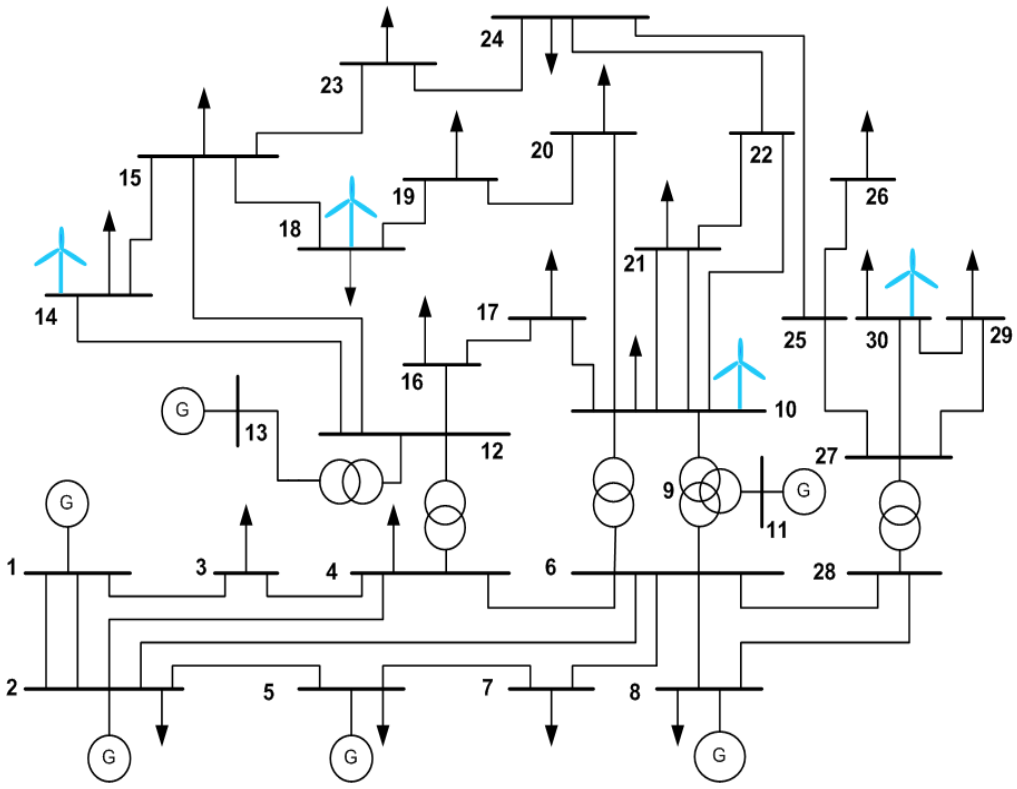

Figure 3: IEEE 30-bus system, including FSIG/DFIG wind farms

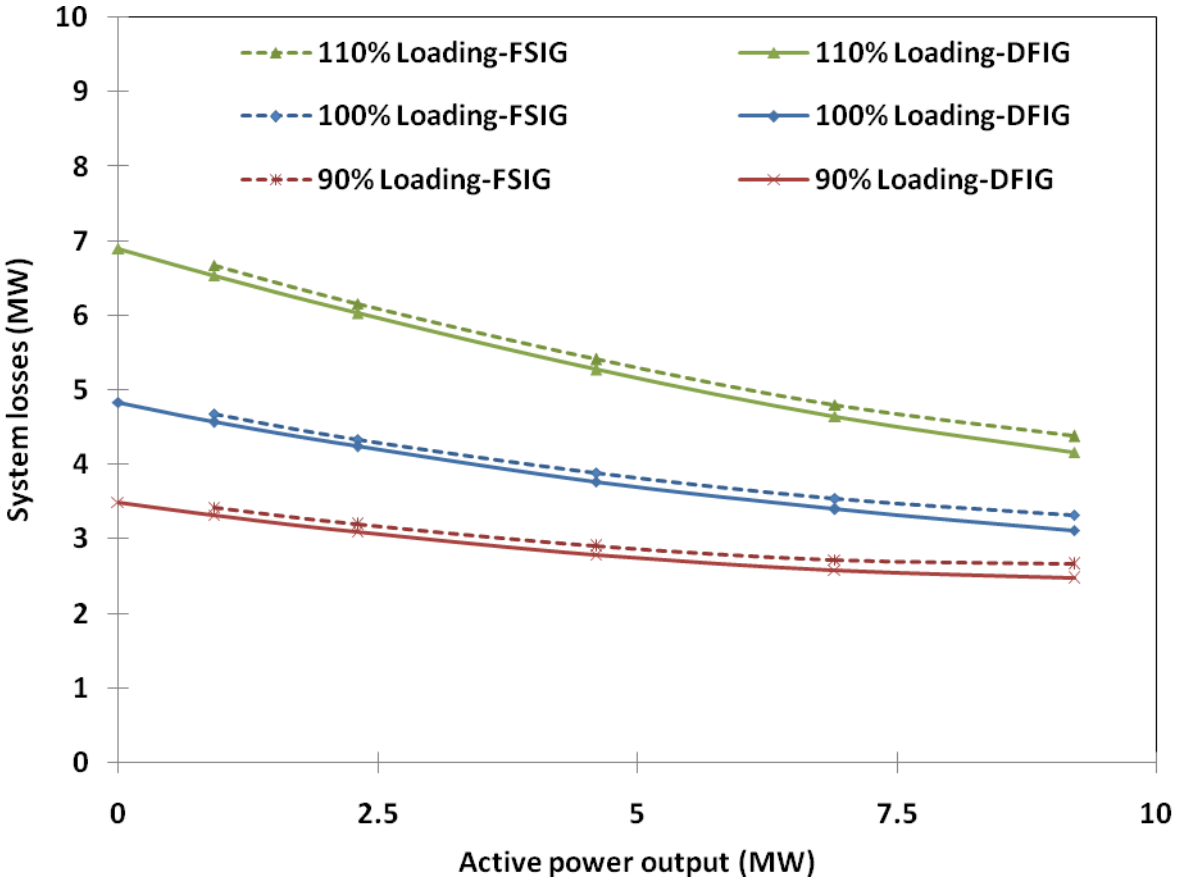

Figure 4: System losses with 4 × 9.2 MW installed wind capacity

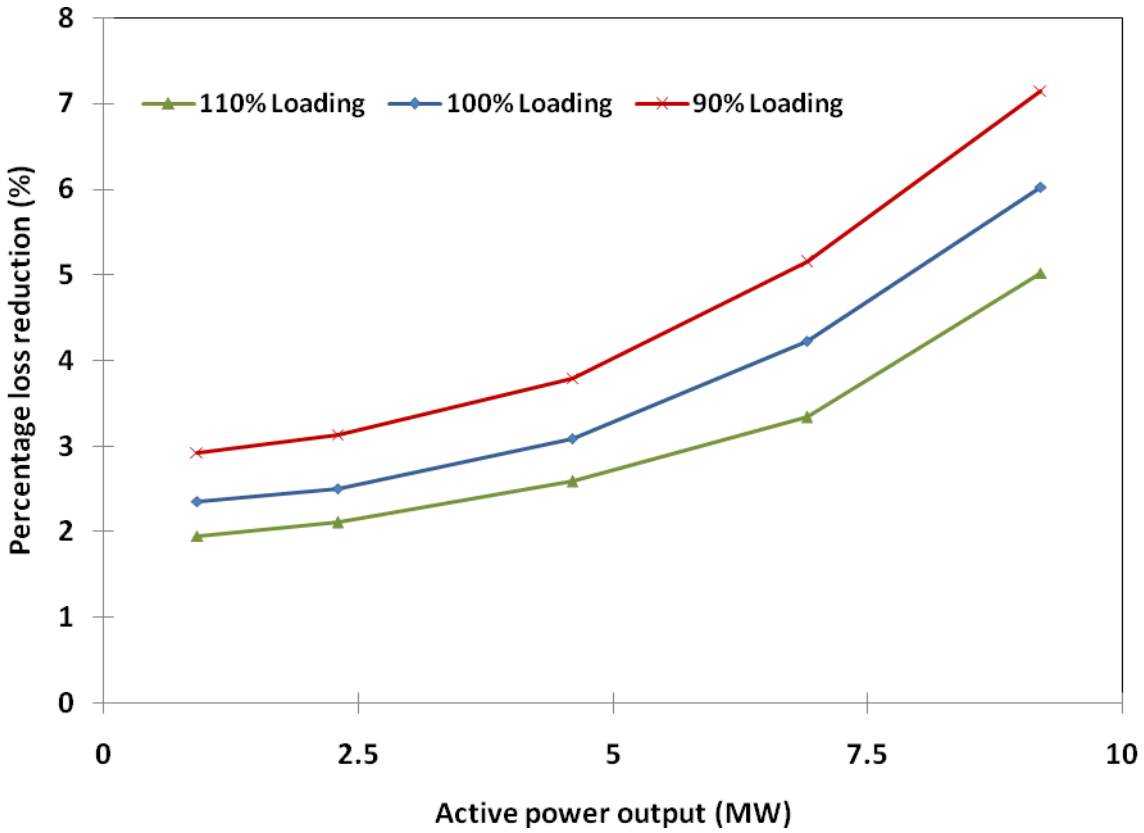

Figure 5: Extra loss reduction with 4 × 9.2 MW of DFIG *cf*. FSIG wind capacity

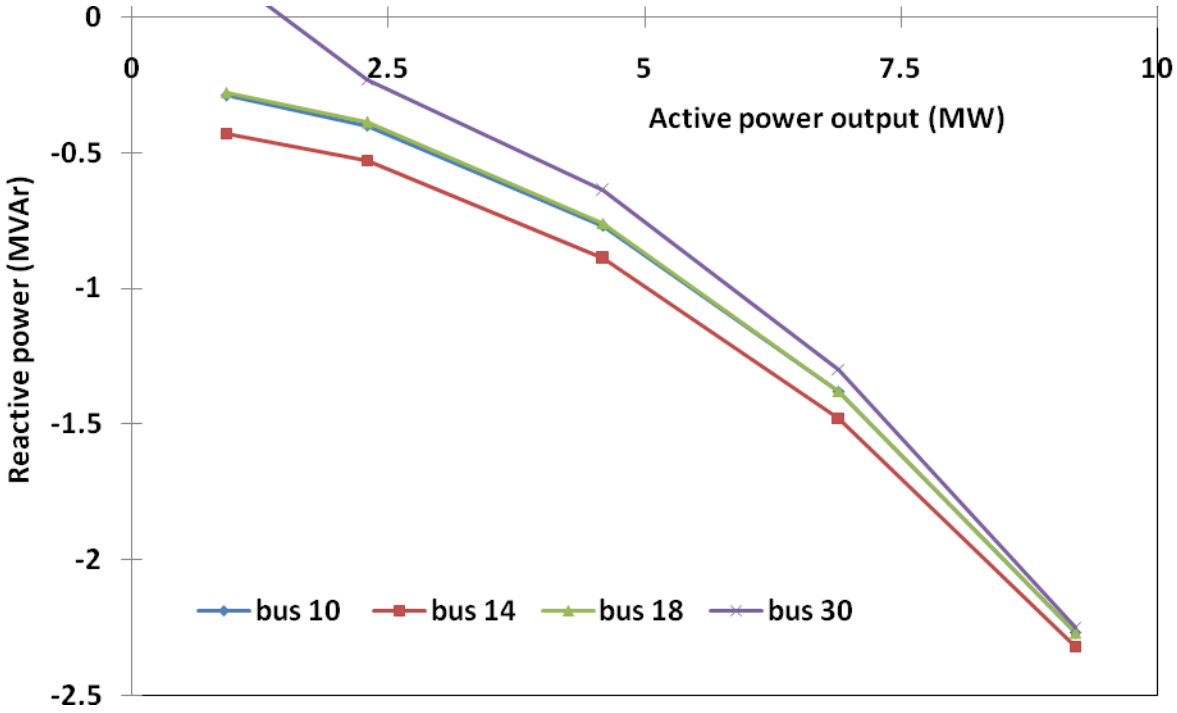

(a)

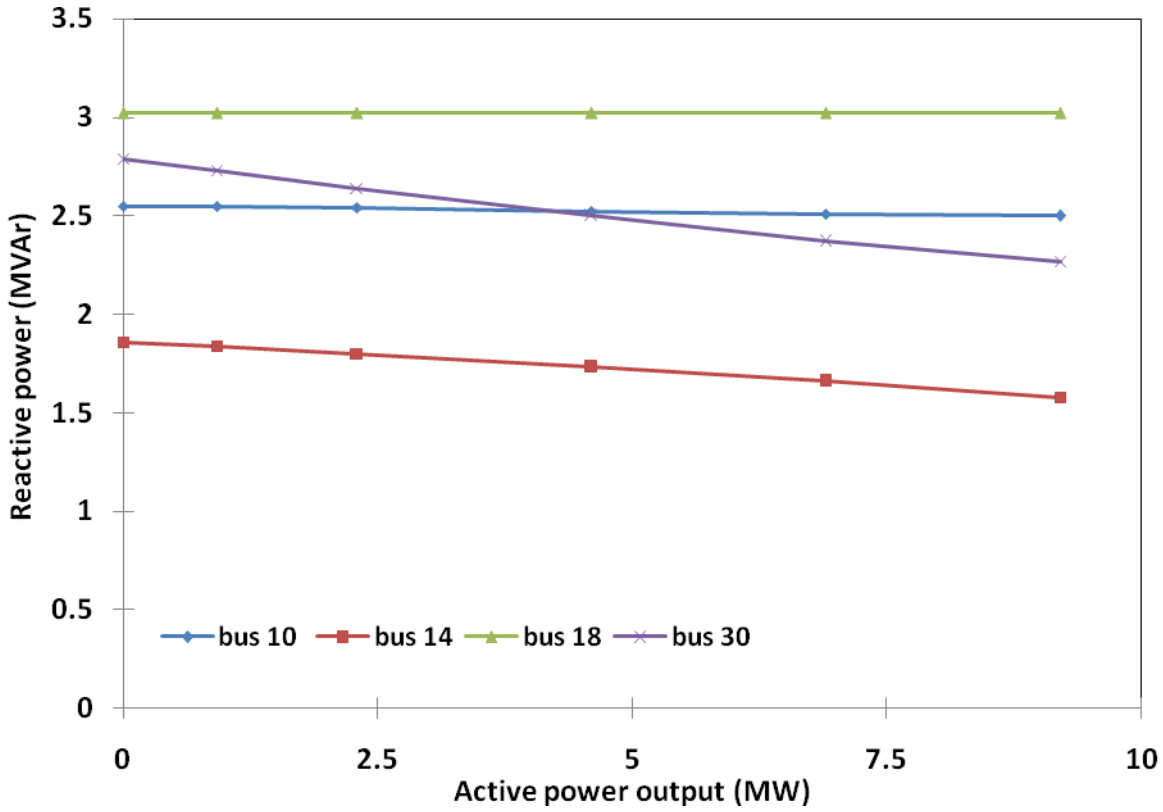

(b)

Figure 6: Net reactive power export for 100% load condition: (a) FSIG, (b) DFIG

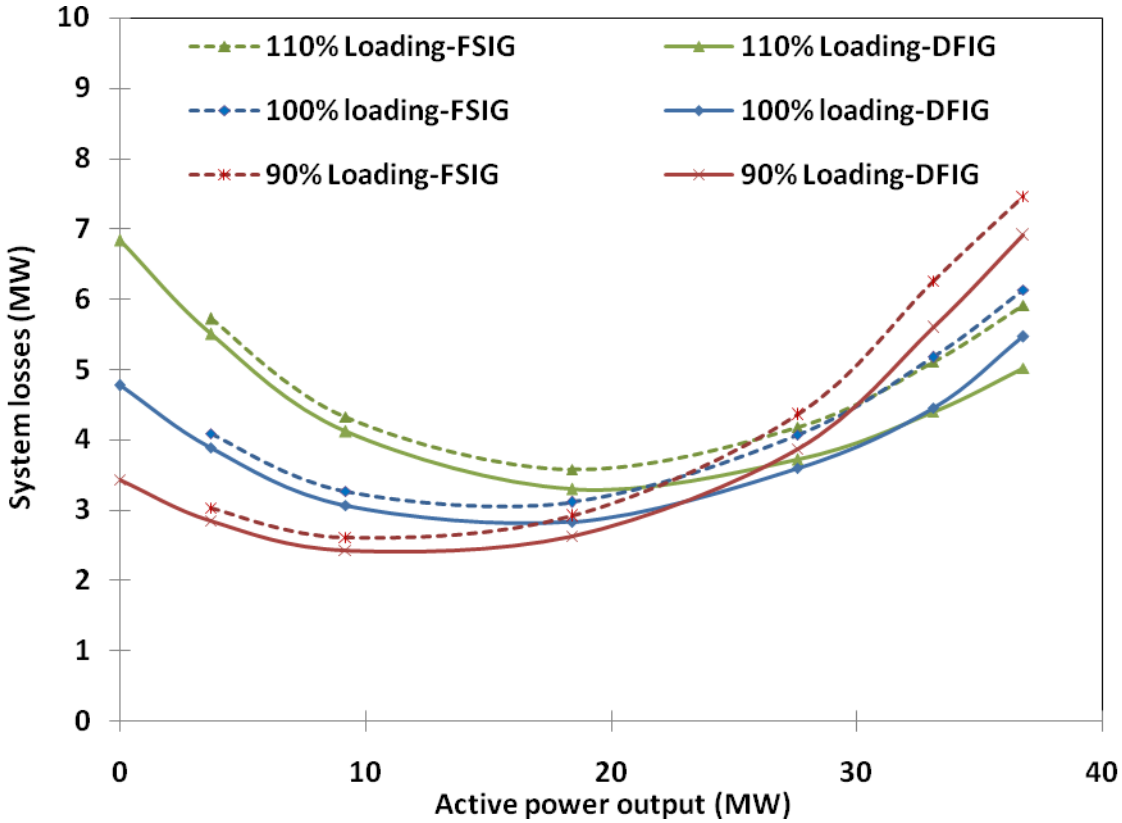

Figure 7: System losses with 4 × 36.8 MW installed wind capacity

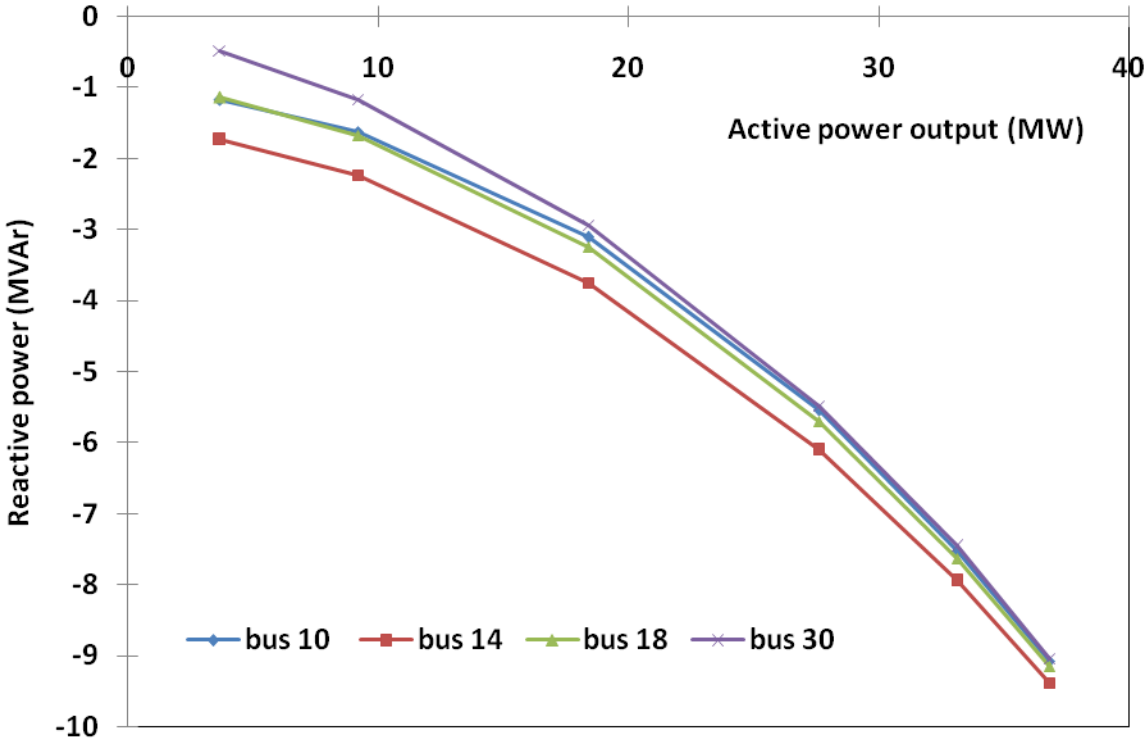

(a)

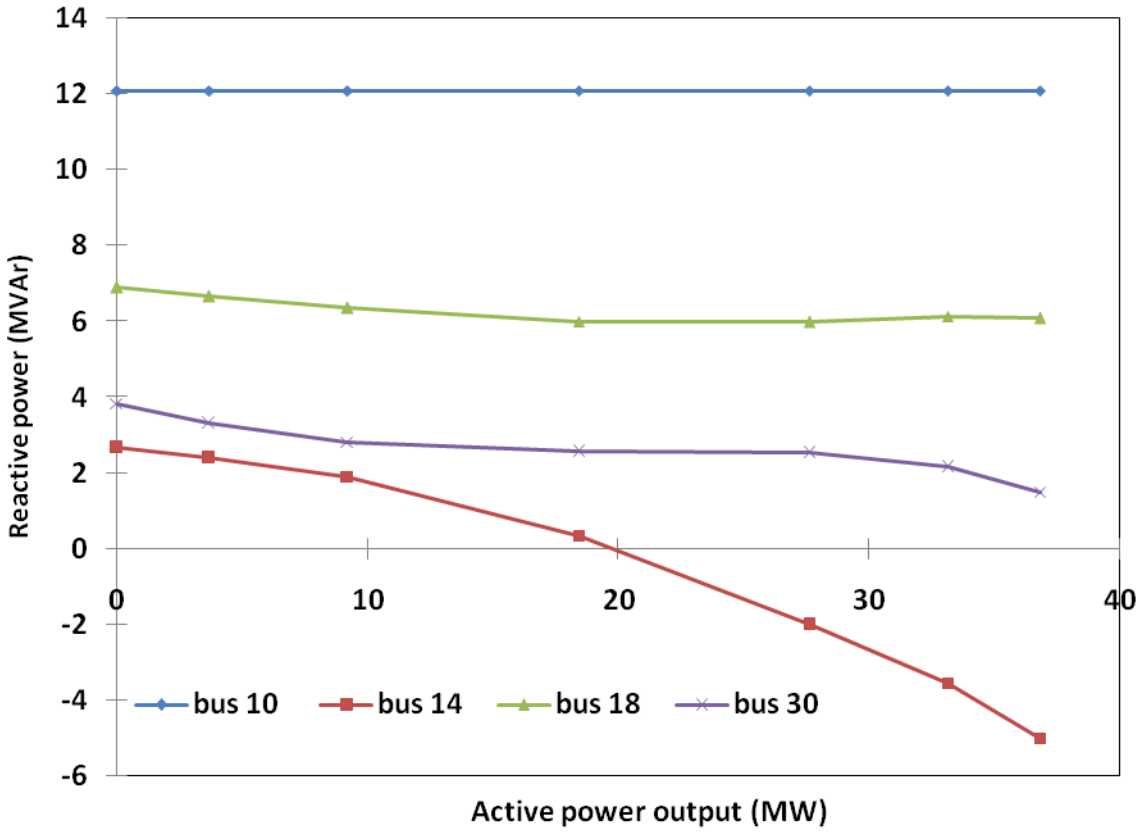

(b)

Figure 8: Net reactive power export for 100% load condition: (a) FSIG, (b) DFIG

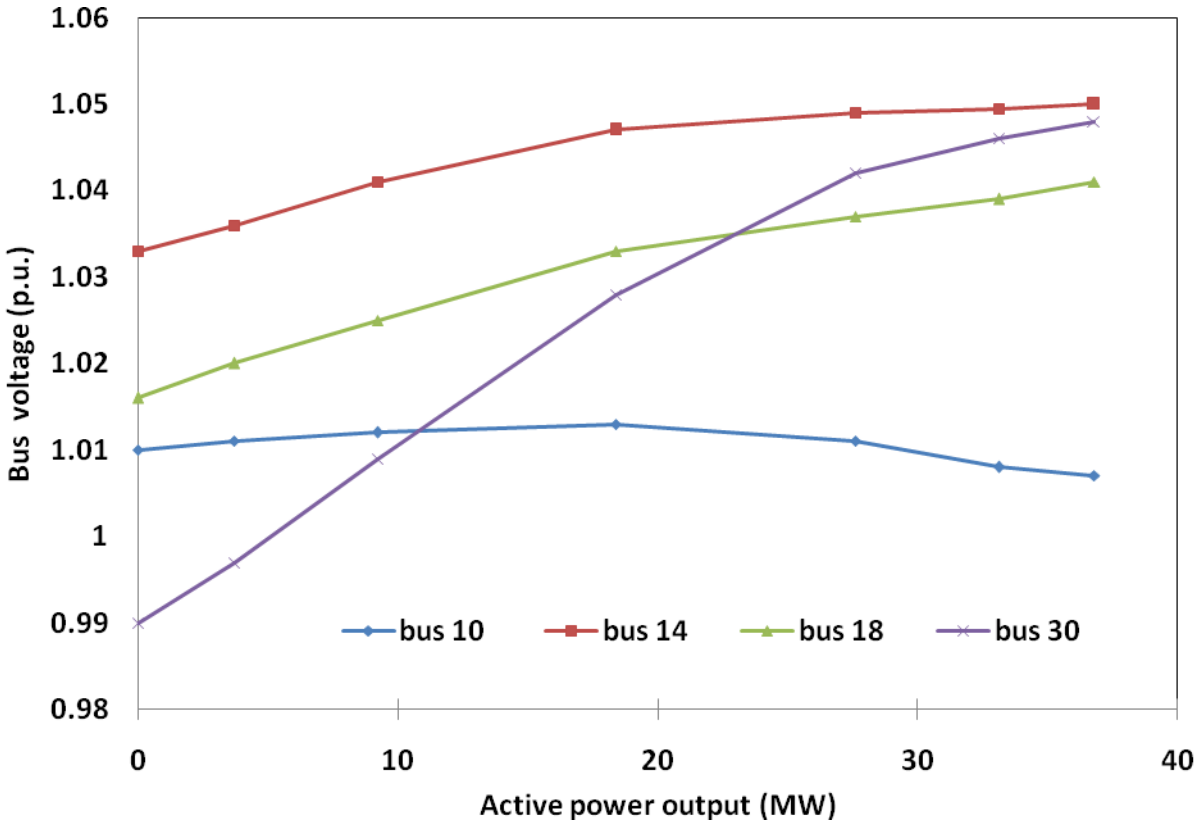

Figure 9: Bus voltages for DFIG technology under 100% load condition

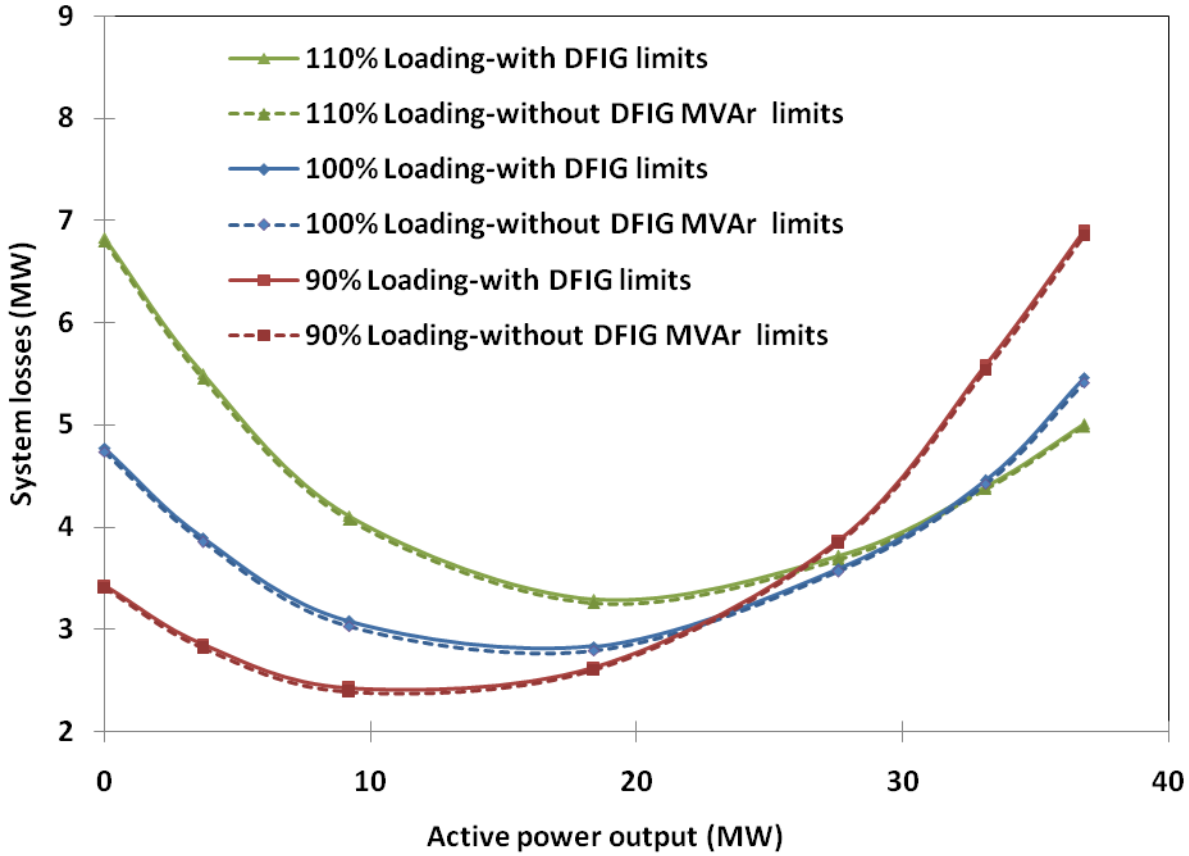

Figure 10: System losses for 0.95 pf/unconstrained converter ratings with 4 × 36.8 MW DFIG installations

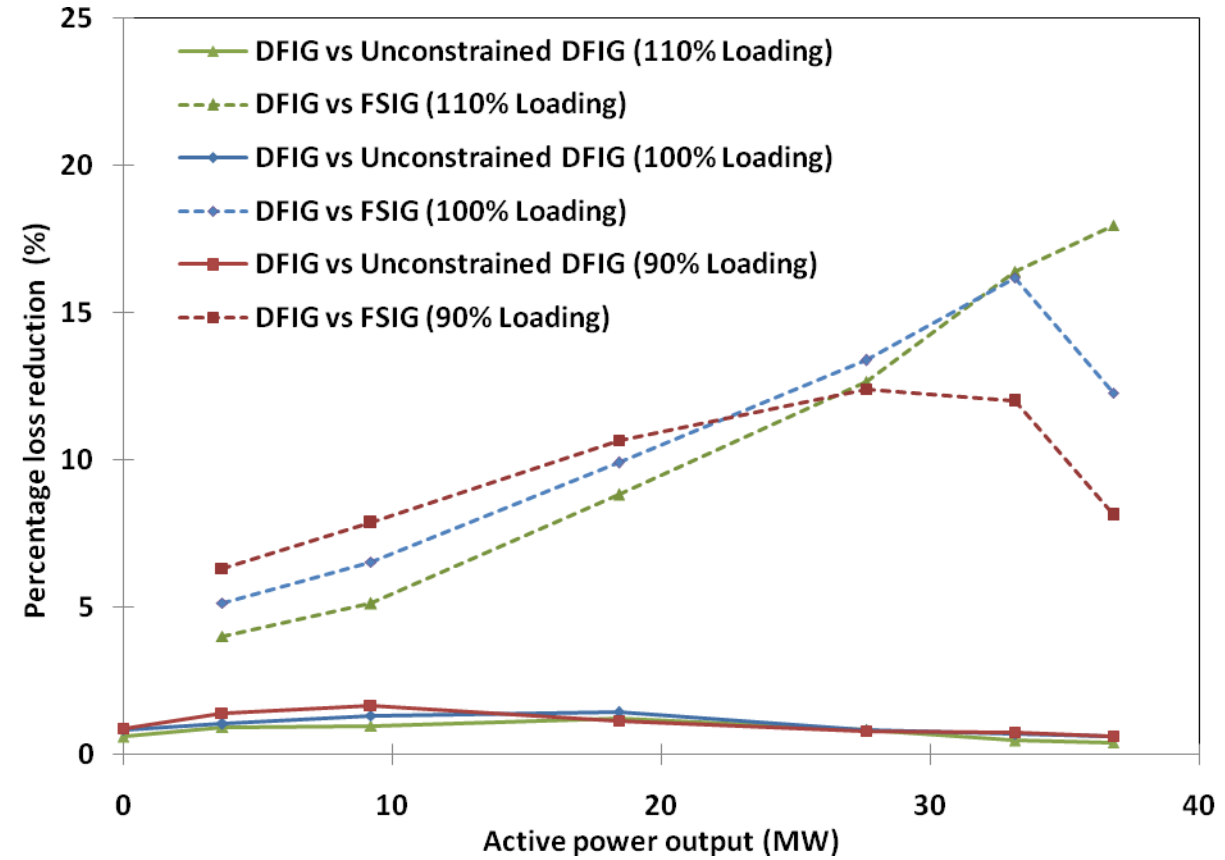

Figure 11: System loss reductions for 4 × 36.8 MW FSIG/DFIG installations

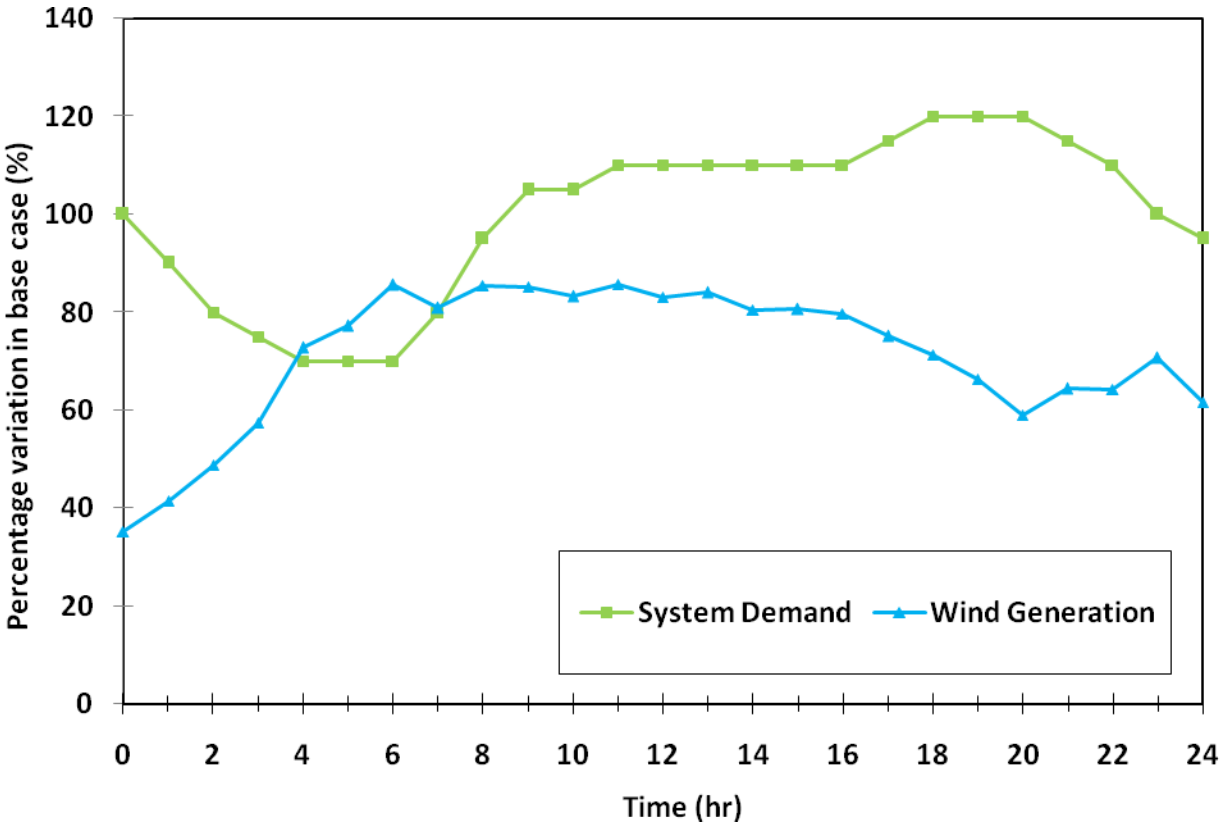

Figure 12: Normalised system demand and wind generation for Ireland system

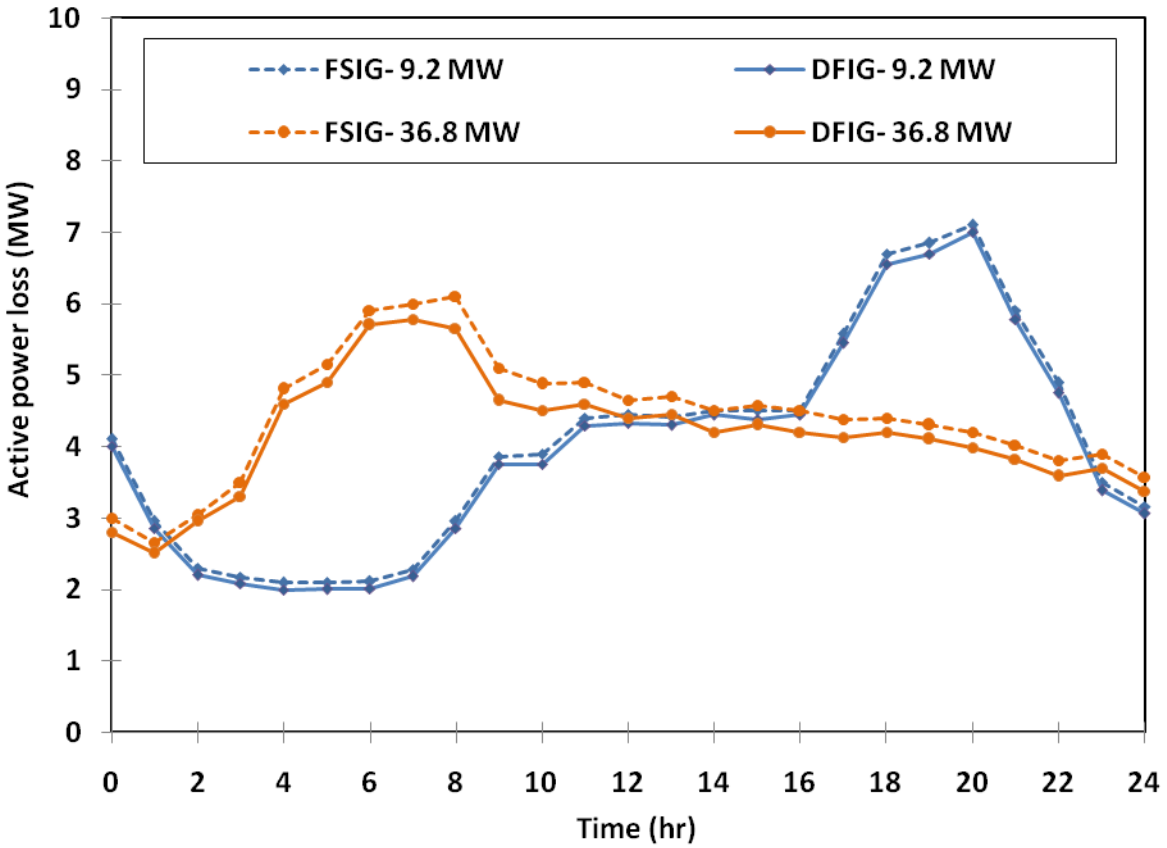

Figure 13: System active power losses for 4 × 9.2/36.8 MW wind farm installations

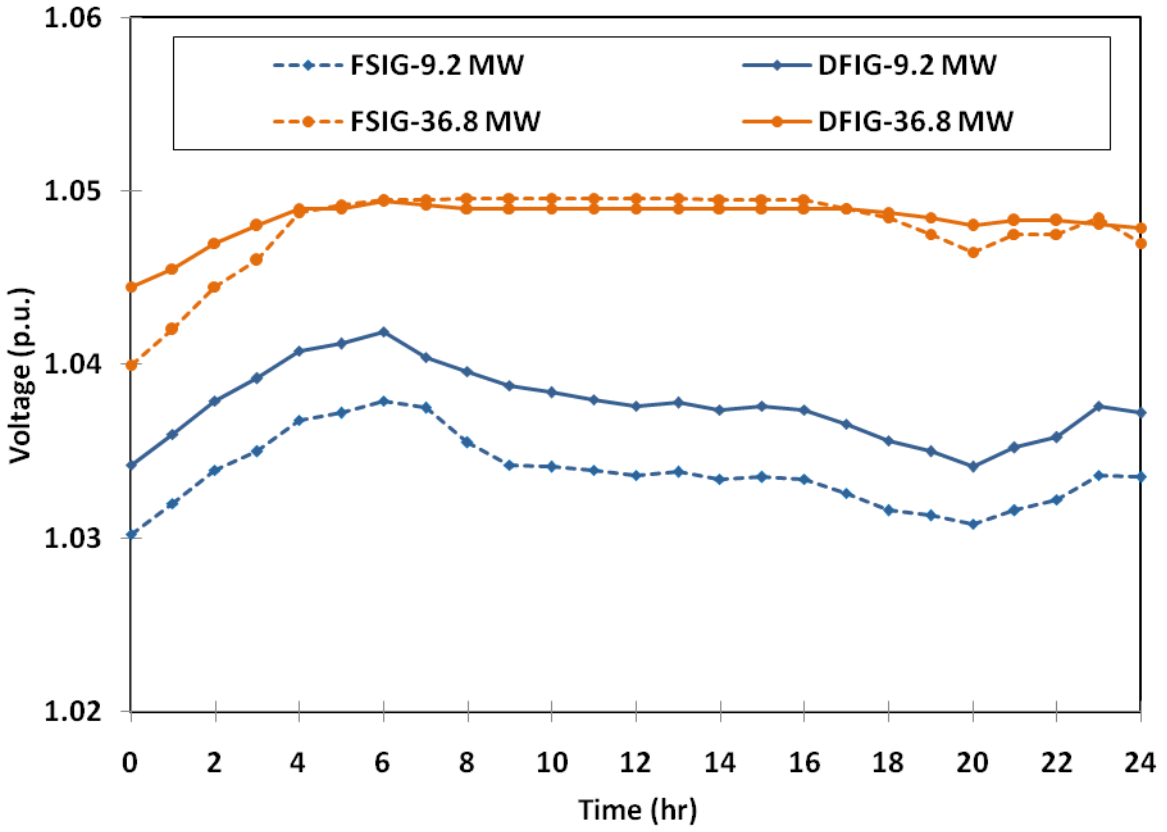

(a)

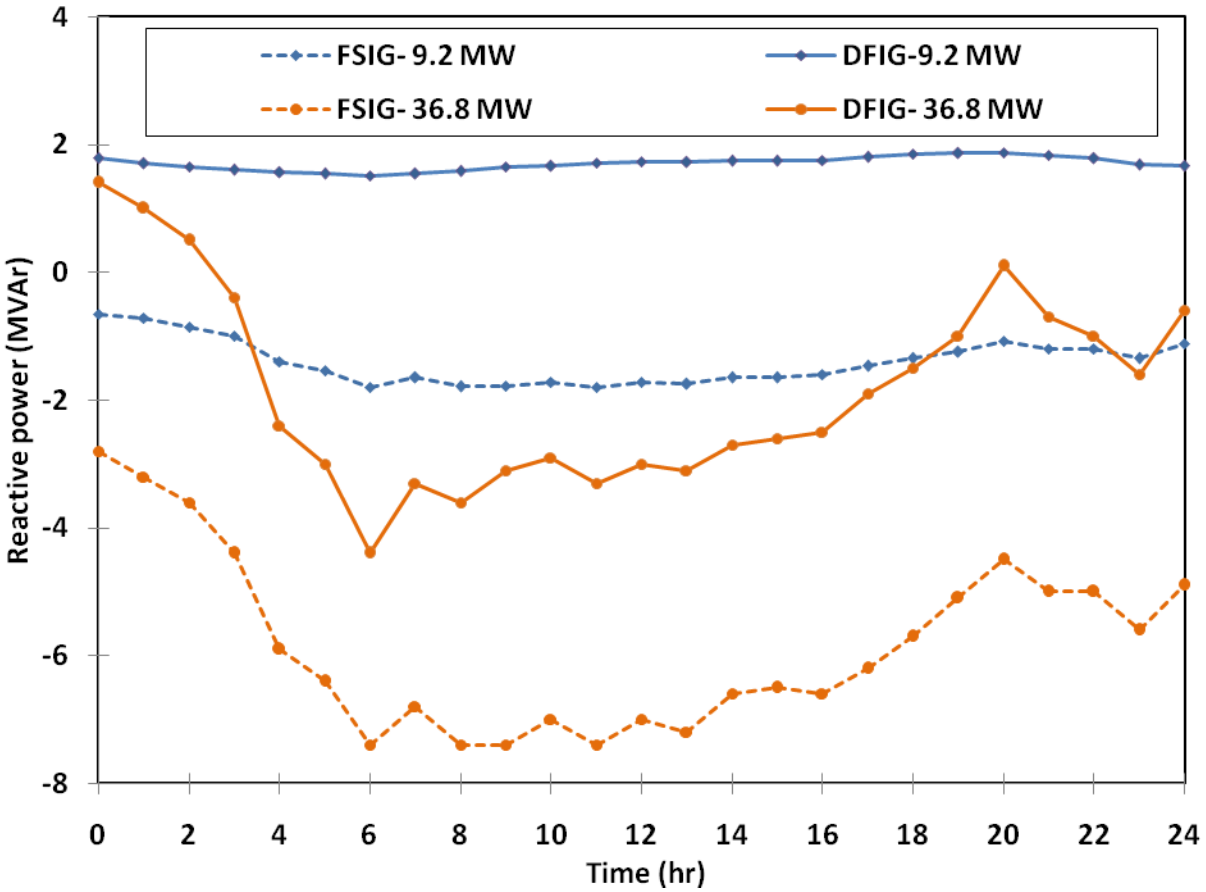

(b)

Figure 14: Bus 14 variations for 4 × 9.2/36.8 MW wind farm installations: (a) voltage, (b) reactive power